Measurements of Friction and Adhesion for Alkyl Monolayers on Si(111) by Scanning Force Microscopy

Luzheng Zhang, Lingyan Li, Shengfu Chen, and Shaoyi Jiang*

Department of Chemical Engineering, University of Washington, Seattle, Washington 98195

Received November 26, 2001. In Final Form: February 25, 2002

In this study, quantitative nanoscale frictional and pull-off forces were measured by scanning force microscopy for various C_{12} alkyl monolayers with different terminal groups ranging from hydrophobic (terminated by $-CH_3$) to hydrophilic (terminated by $-COOH$) on atomically flat Si(111) surfaces at a variety of relative humidities. These monolayers were prepared and characterized by techniques such as scanning probe microscopy, contact angle goniometry, and X-ray photoelectron spectroscopy. The magnitude of the frictional force was found to decrease in the order $SiO_2/Si > -COOH_{Si} > -COOCH_{3,Si} > -CH_{3,Si} \sim -CH_{3,Au}$. On comparison to the native oxide silicon surface, the friction coefficient decreases dramatically when the surface is coated with different monolayers: by 20 times for hydrophobic monolayers and by 3 times for hydrophilic monolayers. Pull-off forces are generally larger for hydrophilic than for hydrophobic surfaces. For hydrophobic surfaces, frictional and pull-off forces are not sensitive to relative humidity. For hydrophilic surfaces, however, friction coefficient decreases while pull-off force increases with increase of relative humidity.

1. Introduction

Friction and adhesion are crucial factors that control the efficiency and durability of moving mechanical assemblies in micro- or nano-electromechanical systems (MEMS/NEMS).[1−3] Self-assembled monolayers (SAMs) are one of the strategies used for minimizing stiction and reducing adhesion and friction in MEMS/NEMS. SAMs on silicon traditionally rely on siloxane chemistry on oxidized surfaces.[1−3] Silane-based monolayers show good stability, but the formed silicon−oxygen bonds are susceptible toward hydrolysis and are thermally labile.[4] Furthermore, the reproducibility of the synthesis of the monolayers is sometimes problematic as well. An alternative approach is a direct thermal reaction between an alkene and an H-terminated silicon surface to form stable organic films via Si−C linkage.[5−14] Other methods, such as electrochemistry, organometallic chemistry, and photoactivation were also applied to prepare the monolayers by forming Si−C linkage.[15−30] Various experimental techniques including scanning probe microscopy (SPM), IR spectroscopy, contact angle goniometry, ellipsometry, X-ray reflectivity, and X-ray photoelectron spectroscopy (XPS) have been used to characterize organic thin films.[31] Molecular mechanics (MM) and molecular dynamics (MD) simulations were performed to study the packing structure of alkyl monolayers on Si(111).[32−34] These new monolayers via Si−C linkage have several key advantages over the

* To whom correspondence should be addressed. Phone: (206) 616-6509. Fax: (206) 685-3451. E-mail: sjiang@u.washington.edu.

(1) (a) Maboudian, R. *Surf. Sci. Rep.* **1998**, *30*, 207−269. (b) Maboudian, R.; Howe, R. T. *J. Vac. Sci. Technol., B* **1997**, *15*, 1−20.
(2) Maboudian, R.; Ashurst, W. R.; Carraro, C. *Sens. Actuators* **2000**, *82*, 219−223.
(3) Jiely, J. D.; Houston, J. E.; Mulder, J. A.; Hsung, R. P.; Zhu, X. Y. *Tribol. Lett.* **1999**, *7*, 103−107.
(4) Calistri-Yeh, M.; Kramer, R. J.; Sharma, R.; Zhao, W.; Rafailovich, M. H.; Sokolov, J.; Brock, J. D. *Langmuir* **1996**, *12*, 2747−2755.
(5) Linford, M. R.; Fenter, P.; Eisenberger, P. M.; Chidsey, C. E. D. *J. Am. Chem. Soc.* **1995**, *117*, 3145−3155.
(6) Terry, J.; Linford, M. R.; Wigren, C.; Cao, R.; Pianetta, P.; Chidsey, C. E. D. *J. Appl. Phys.* **1999**, *85*, 213−221.
(7) Cicero, R. L.; Linford, M. R.; Chidsey, C. E. D. *Langmuir* **2000**, *16*, 5688−5695.
(8) Sieval, A. B.; Demirel, A L.; Nissink, J. W. M.; Linford, M. R.; van der Maas, J. H.; de Jeu, W. H.; Zuilhof, H.; Sudholter, E. J. R. *Langmuir* **1998**, *14*, 1759−1768.
(9) Sieval, A. B.; Linke, R.; Zuilhof, H.; Sudholter, E. J. R. *Adv. Mater.* **2000**, *12*, 1457−1460.
(10) Sieval, A. B.; Vleeming V.; Zuilhof, H.; Sudholter, E. J. R. *Langmuir* **1999**, *15*, 8288−8291.
(11) Sieval A. B.; Optiz, R.; Maas, H. P. A.; Schoeman, M. G.; Frank, G. M.; Vergeldt, F. J.; Zuilhof, H.; Sudgolter, E. J. R. *Langmuir* **2000**, *16*, 10359−10368.
(12) Sung, M. M.; Kluth, G. J.; Yauw, O. W.; Maboudian, R. *Langmuir* **1997**, *13*, 6164−6168.
(13) Ashurst, W. R.; Yan, C.; Carraro, C.; Howe, R. T.; Maboudian, R. *Proceedings of solid-state sensor and actuator workshop*, Hilton Head 2000, Hilton Head Island, SC, pp 320−323.
(14) Bateman, J. E.; Eagling, R. D.; Worrall, D. R.; Horrocks, B. R.; Houlton, A. *Angew. Chem., Int. Ed.* **1998**, *37*, 2683−2685.
(15) Royea, W. J.; Juang, A.; Lewis, N. S. *Appl. Phys. Lett.* **2000**, *77*, 1988−1990.
(16) Bansal, A.; Lewis, N. S. *J. Phys. Chem. B* **1998**, *102*, 1067−1070.
(17) Bansal, A.; Lewis, N. S. *J. Phys. Chem. B* **1998**, *102*, 4058−4060.
(18) Boukherroub, R.; Morsin, S.; Bensebaa, F.; Wayner, D. D. M. *Langmuir* **1999**, *15*, 3831−3835.
(19) Boukherroub, R.; Morsin, S.; Sharpe, P.; Wayner, D. D. M. *Langmuir* **2000**, *16*, 7429−7434.
(20) Boukherroub, R.; Wayner, D. D. M. *J. Am. Chem. Soc.* **1999**, *121*, 11513−11515.
(21) Lopinski, G. P.; Wayner, D. D. M.; Wolkow, R. A. *Nature* **2000**, *406*, 48−51.
(22) de Villeneuve, C. H.; Pinson, J.; Bernard, M. C.; Allongue, P. *J. Phys. Chem. B* **1997**, *101*, 2415−2420.
(23) Allongue, P.; Delamar, M.; Debat, B.; Fagebaume, O.; Hitmi, R.; Pinson, J.; Saveant, J.-M. *J. Am. Chem. Soc.* **1997**, *119*, 201−207.
(24) Allongue, P.; de Villeneuve, C. H.; Pinson, J.; Ozanam, F.; Chazalviel, J. N.; Wallart, X. *Electrochim. Acta*, **1998**, *43*, 2791−2798.
(25) Effenberger, F.; Gotz, G.; Bidlingmaier, B.; Wezstein, M. *Angew. Chem., Int. Ed.* **1998**, *37*, 2462−2464.
(26) Padowitz, D. F.; Hamers, R. J. *J. Phys. Chem. B* **1998**, *102*, 8541−8545.
(27) Hamers, R. J.; Hovis, J. S.; Coulter, S. K.; Ellison, M. D.; Padowitz, D. F. *Jpn. Appl. Phys.* **2000**, *39*, 4366−4371.
(28) Buriak, J. M. *Chem. Commun.* **1999**, 1051−1060.
(29) Stewart, M. P.; Buriak, J. M. *Adv. Mater.* **2000**, *12*, 859−869.
(30) Buriak, J. M.; Stewart, M. P.; Geders, T. W.; Allen, M. J.; Choi, H. C.; Smith, J.; Raftery, D.; Canham, L. T. *J. Am. Chem. Soc.* **1999**, *121*, 11491−11502.
(31) Vickerman, J. C. *Surface Analysis−The principal Techniques*; Wiley: New York, 1997.
(32) Sieval, A. B.; van der Hout, B.; Zuilhof, H.; Sudholter, E. J. R. *Langmuir* **2000**, *16*, 2987−2990.
(33) Sieval, A. B.; van der Hout, B.; Zuilhof, H.; Sudholter, E. J. R. *Langmuir* **2001**, *17*, 2172−2181.
(34) Zhang, L.; Wesley, K.; Jiang, S. *Langmuir* **2001**, *17*, 6275−6381.

10.1021/la011718a CCC: $22.00
Published on Web 06/13/2002

Table 1. Summary of Surfaces Used in This Work, Preparation Methods, and Advancing Water Contact Angles

surface	preparation method	contact angle (deg)
CH_2═$CH-(CH_2)_9-CH_3$/Si(111)	thermal reaction	104
CH_2═$CH-(CH_2)_8-COOCH_3$/Si(111)	thermal reaction	55
CH_2═$CH-(CH_2)_8-COOH$/Si(111)	hydrolysis in acid solution	48
native oxide silicon	cleaned by UV	27
hydrogen terminated Si(111)	etched in 40% NH_4F solution	79
C_{12} alkanethiol/Au(111)	self-assembly	107

previously reported silane-based SAMs:[13] (i) The coating does not produce HCl. (ii) The coating does not require the formation of an intervening oxide layer. (iii) The film formation procedure is simpler. (iv) The coating process is much more robust. (v) The coated surface has fewer particulates. (vi) The film is stable up to 615 K.[12] The direct reaction between alcohols and H-terminated[35,36] or Cl-terminated[37] silicon has also been proposed to form stable organic films via Si−O linkage.

Scanning force microscopy (SFM) is an ideal instrument to study the phenomena down to the atomic scale. The advantage of the SFM is that it allows the accurate measurements of forces applied in the horizontal as well as normal directions to a surface. It has been observed that frictional force of alkanethiols on Au(111) decreases as the chain length of thiols increases from C_8 to C_{18}[38−40] or as the size of terminal groups decreases from $-CF_3$ to $-CH_3$ [41] and that frictional force depends on scan direction.[42,43] The application of SFM in the study of frictional properties has been carried out on silanes[39,44−46] and alkanethiol/Au(111) with chemically modified tips.[45−49] Recently, a humidity effect on frictional properties of SAMs has been studied by Li et al.,[50] Leggett et al.,[51] and Tian et al.[52] So far, there is still a considerable lack of the fundamental understanding of adhesion and friction at the molecular level. To the best of our knowledge, no SFM measurements of nanoscale friction and adhesion for alkyl monolayers on silicon were reported previously.

In this work, C_{12} alkyl monolayers with different terminal groups ranging from hydrophobic ($-CH_3$) to hydrophilic ($-COOH$) on an atomically flat Si(111) surface were prepared and characterized by SPM, contact angle goniometry, and XPS. Nanoscale frictional forces for these monolayers and pull-off forces were measured using SFM at a variety of relative humidities.

2. Experiments

2.1. Materials. 1-Dodecene ($C_{12}H_{24}$, 99.5%), undecylenic acid methyl ester ($C_{12}H_{22}O_2$, 99%), and other organic materials for cleaning and rinsing were purchased from Sigma-Aldrich (St. Louis, MO); ammonium fluoride (NH_4F, 99.8%) was purchased from J. T. Baker (Phillipsburg, NJ). All chemicals were used as received. House-distilled water was passed through a purification unit to produce deionized (DI) water with a resistivity of 18.0 MΩ cm. Si(111) wafers (432 μm thickness) were purchased from Virginia Semiconductor (Fredericksburg, VA).

2.2. Monolayer Preparation. *The basic and acidic solutions of hydrogen peroxide described in this procedure are exceedingly dangerous and should be handled with great care.* Silicon samples (6 mm × 8 mm) were cut from Si(111) wafers using a diamond blade. The samples were cleaned for 30 min in ∼100 °C 3:1 H_2SO_4 (concentrated)/30% H_2O_2 by volume and for 30 min in ∼100 °C 6:1:1 H_2O/HCl (concentrated)/30% H_2O_2. The silicon surfaces were rinsed thoroughly with DI water after each cleaning step and dried by a stream of nitrogen. Hydrogen-terminated Si(111) surfaces were formed by etching the cleaned silicon surface in a degassed (at least 1 h) 40% NH_4F aqueous solution for 5 min, followed by water rinsing and nitrogen blow drying. The hydrogen-terminated Si(111) surfaces were then dipped into a small flask containing ∼3 mL neat solution of precursors (either 1-dodecene or undecylenic acid methyl ester in this work). The solution was degassed by nitrogen and then heated to 200 °C for 2 h, while nitrogen was slowly bubbled through the solution. The solution temperature was controlled within ±1 °C by a home-built oil bath. Subsequently, the silicon pieces were removed from the solution after they cooled to room temperature, rinsed three times in petroleum ether (∼50 °C), 2-propanol, and dichloromethane, respectively, sonicated in dichloromethane, and dried in a stream of nitrogen. The prepared samples were stored in microtubes filled with nitrogen. The carboxyl-terminated ($-COOH$) monolayers were generated by a hydrolysis reaction of ester-terminated ($-COOCH_3$) monolayers in the presence of acid. The ester-terminated monolayer was dipped into a boiling H_2SO_4 aqueous solution (∼0.2 M) for 1−2 h, washed with DI water, and dried by nitrogen. The surfaces used in this work are listed in Table 1. The methyl-terminated monolayer ($C_{11}-CH_3$/Si) is abbreviated to $-CH_{3,Si}$, the ester-terminated monolayer ($C_{10}-COOCH_3$/Si) to $-COOCH_{3,Si}$, the carboxyl-terminated monolayer ($C_{10}-COOH$/Si) to $-COOH_{,Si}$, the C_{12} alkanethiol monolayer on Au(111) to $-CH_{3,Au}$, and the hydrogen-terminated Si(111) surface to H−Si.

2.3. Surface Characterizations. AFM and STM. The SPM technique includes atomic force microscopy (AFM), friction force microscopy (FFM), scanning tunneling microscopy (STM), and so on.[53,54] The techniques based on force measurements, such as AFM and FFM, also are referred to as SFM. A multimode SPM (Digital Instrument, Santa Barbara, CA) was used to characterize the topography of H−Si and alkyl monolayers in the contact mode. STM (OMICRON Vakuumphysik GmbH, Germany) was also used to obtain the topography of a H−Si surface in a constant-current mode. The gap voltage for STM was −2.1 V.

(35) Cleland, G.; Horrocks, B. R.; Houlton, A. *J. Chem. Soc., Faraday Trans.* **1995**, *91*, 4001−4003.
(36) Bateman, J. E.; Eagling, R. D.; Horrocks, B. R.; Houlton, A. *J. Phys. Chem. B* **2000**, *104*, 5557−5565.
(37) Zhu, X.-Y.; Boiadjiev, V.; Mulder J. A.; Hsung, R. P.; Major R. C. *Langmuir* **2000**, *16*, 6766−6772.
(38) Li, L.; Yu, Q.; Jiang, S. *J. Phys. Chem. B* **1999**, *103*, 8290−8295.
(39) Lio, A.; Charych, D. H.; Salmeron, M. *J. Phys. Chem. B* **1997**, *101*, 3800−3805.
(40) McDermott, M. T.; Green, J.-B. D.; Porter, M. D. *Langmuir* **1997**, *13*, 2504−2510.
(41) Kim, H. I.; Koini, T.; Lee, T. R.; Perry, S. S. *Langmuir 1997*, 13, 7192−7196.
(42) Last, J. A.; Ward, M. D. *Adv. Mater.* **1996**, *8*, 730.
(43) Schonherr, H.; Kenis, P. J. A.; Engbersen, J. F. J.; Harkema, S.; Hulst, R.; Reinboudt, D. N.; Vancso, G. J. *Langmuir* **1998**, *14*, 2801−2809.
(44) Liu, Y.; Wu, T.; Evans, D. F. *Langmuir* **1994**, *10*, 2241−2245.
(45) Clear, S. C.; Nealey, P. F. *J. Colloid Interface Sci.* **1999**, *213*, 238−250.
(46) Moser, A.; Eckhardt, C. J. *Thin Solid Films* **2001**, *382*, 202−213.
(47) (a) Frisbie, C. D.; Tozsnyai, L. F.; Noy, A.; Wrighton, M. S.; Lieber, C. M. *Science* **1994**, *265*, 2071−2074. (b) Noy, A.; Frisbie, C. D.; Rozsnyai, L. F.; Wrighton, M. S.; Lieber, C. M. *J. Am. Chem. Soc.* **1995**, *117*, 7943−7951.
(48) Green, J.-B. D.; McDermott, M. T.; Porter, M. D.; Siperko, L. M. *J. Phys. Chem.* **1995**, *99*, 10960−10965.
(49) Fujihira, M.; Tani, Y.; Furugoti, M.; Akiba, U.; Okabe, Y. *Ultramicroscopy* **2001**, *86*, 63−73.
(50) Li, L.; Chen, S.; Jiang, S. (Frommer J. E. and Overney, R. Eds.) *ACS Symp. Ser.* **2001**, 168−177.
(51) Brewer, N. J.; Beake, B. D.; Leggett, G. J. *Langmuir* **2001**, *17*, 1970−1974.
(52) Tian, F.; Xiao, X.; Loy, M. M. T.; Wang, C.; Bai, C. *Langmuir*, **1999**, *15*, 244−249.
(53) Binnig, G.; Quate, C. F.; Gerber, C. *Phys. Rev. Lett.* **1986**, *56*, 930−933.
(54) Mate, C. M.; McClelland, G. M.; Erlandsson, R.; Chiang, S. *Phys. Rev. Lett.* **1987**, *59*, 1942−1945.

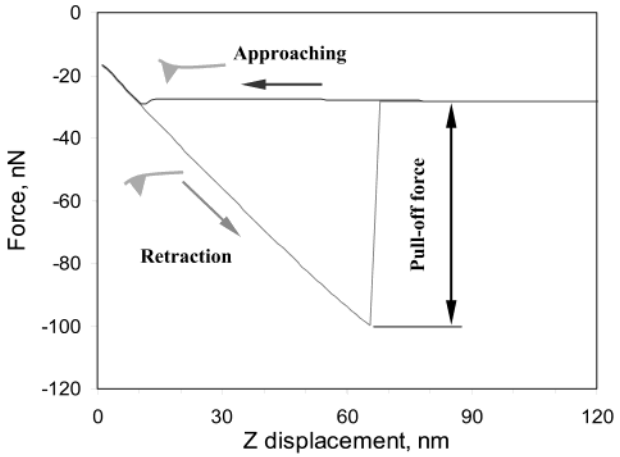

Figure 1. Typical approach/retraction cycle in a friction measurement by scanning force microscopy.

Contact Angle. Contact angles for water were measured with a tensiometer (Ramé-Hart Inc., Mountain Lakes, NJ). The samples were horizontally placed on a stage and 2 μL of water was dropped on the top of the samples. At least three measurements were made for each sample. The uncertainty of measurements was about $\pm 1°$.

XPS Analysis. XPS spectra were obtained on a Surface Science Instruments X-probe and M-probe spectrometers equipped with a Monochromatic Al Kα X-ray sources ($h\nu$ = 1486.6 eV), hemispherical electron analyzer, and channel plate/resistive strip anode detectors. Cryopumped ultrahigh vacuum (UHV) analysis chambers provide base pressures below 1×10^{-9} Torr. Computer-controlled XYZ-theta sample manipulators in the analysis chambers were used for automated data acquisition. All XPS data were acquired at a nominal photoelectron takeoff angle of 55°, where the takeoff angle is defined as the angle between the surface normal and the axis of the analyzer lens. Spectra of C(1s) (275−295 eV binding energy) and Si(2p) (90−110 eV) as well as survey scans (0−1000 eV) were recorded.

2.4. Friction Measurement by SFM. Friction measurements were carried out with the multimode SPM. Commercially available 100-μm-long, 36-μm-wide, gold-coated, V-shaped Si_3N_4 cantilevers with a nominal force constant of 0.58 N/m (Digital Instruments) were used. The microscope was operated in the constant-load mode. A home-built chamber was used to keep relative humidity constant with an uncertainty of $\pm 1\%$. The humidity was controlled by injecting either dry nitrogen or water-saturated nitrogen into the chamber. Experimental measurements were performed from high to low humidity. To minimize the thermal drift, the instrument was allowed to equilibrate inside the chamber for 3−4 h before any data were collected. The temperature inside the chamber was about 28 °C. The piezo scanner sensitivity for the *x*, *y*, and *z* directions was calibrated by the same method as used previously.[38]

To measure frictional forces, two forces were collected, i.e., lateral force from a friction loop and normal force from a force−distance curve. Frictional force is determined by averaging the lateral forces from each of "trace" and "retrace" curves in a friction loop.[38] A force−distance curve is shown in Figure 1. The cantilever is bent up during approach, while it is bent down during retraction. When the tip overcomes adhesion force from the surface, the cantilever restores its original state. The pull-off force is the force jump during retraction. Large-scale topographical images of the SAMs (500 nm × 500 nm) were captured to determine the monatomic terraces. Frictional and pull-off forces were measured within a uniform area of 50 nm × 50 nm on the terrace. The 50-nm trace−retrace cycle of a friction loop showed the sawtooth behavior. The scan rate was ~600 nm/s. The normal force signals between tip and sample, $F_{N,0}$, were determined from the ASCII files of the normal force signal versus *z*-displacement curves. The frictional signals, $F_{L,0}$, were collected from the ASCII files of the friction loops. Measurements were collected for each load for three times.

2.5. Force Calibration. Quantitative nanoscale force measurements with SFM require an accurate calibration of both lateral and normal forces. To convert experimental normal ($F_{N,0}$) and lateral ($F_{L,0}$) deflection signals in voltage into normal (F_N) and lateral (F_L) forces in newtons, one has to obtain lateral and normal force calibration factors (α and β) in units of nN/V

$$F_N = k_N \Delta z = k_N c_N F_{N,0} = \beta F_{N,0}$$

$$F_L = k_L \Delta x = k_L c_L F_{L,0} = \alpha F_{L,0} \quad (1)$$

where k_N and k_L are normal and lateral force constants, Δz and Δx normal and lateral displacements of the cantilever, and c_N and c_L normal and lateral force optical deflection sensitivities. Li et al.[38] combined the two-slope[55] and added mass[56] methods to obtain the calibration factors α and β. The ratio α/β was determined by the two-slope method. The k_N was determined using the added mass method. The c_N was determined by measuring the slope of the normal force signal versus *z*-displacement curve on a hard surface. In this work, a tip of the same type was used to measure the friction of alkanthiol/Au(111), $-CH_{3,Au}$, as used previously.[38] A very close agreement was obtained. Thus, the ratio α/β of 38.5 calibrated previously[38] was used to calculate friction coefficients in this work.

3. Results and Discussion

3.1. Characterization of Monolayers. Hydrogen-Terminated Si(111). The flat Si(111) (1 × 1) surface is capped with only one hydride to satisfy the tetravalency of the silicon atoms, whereas Si(100) (1 × 1) is capped with more than one hydride. H−Si surfaces prepared by standard wet chemical treatments in fluoride solutions are among the best substrates to start with because they can be prepared flat at the atomic level and are chemically homogeneous.[57−60] Thus, a Si(111) surface was used in this work. Figure 2a shows an AFM image of the Si(111) surface after etching in a 40% NH_4F aqueous solution for 5 min. Atomically flat terraces (120 × 120 nm or larger) are observed on the surface. A section analysis of Figure 2a is presented in Figure 2c. The distance between two Si(111) terraces is 0.32 nm, which agrees quite well with the theoretical value of 0.314 nm from its crystal structure. It was shown that etching Si(111) samples in the NH_4F aqueous solution could result in large atomically flat terraces on the surface.[60] Before Si(111) samples were etched, NH_4F aqueous solution was degassed to remove dissolved oxygen by flowing a stream of nitrogen for at least 1 h since oxygen in the etching solution plays an important role in generating large terraces. Chidsey and co-workers[60] have shown that the NH_4F solution without degassing resulted in many small triangle pits on the etched Si(111) surface. This finding was also confirmed in this work. STM was used to characterize the H−Si-(111) surface under ultrahigh vacuum (UHV) conditions. The atomically flat large terraces were also observed from the STM image, as shown in Figure 2b. These H−Si surfaces with large terraces were used for the formation of alkyl monolayers.

When Si(111) surface was terminated by hydrogen after being etched in NH_4F solution, the water contact angle for the surface changed from 27° to 80°. Since the H−Si surface was easily contaminated when exposed to air as observed by AFM, the sample was put into a precursor

(55) Ogletree, D. F.; Carpick, R. W.; Salmeron, M. *Rev. Sci. Instrum.* **1996**, *67*, 3298−3306.
(56) Stokey, W. F. *Shock and Vibration Handbook*; McGraw-Hill: New York, 1989.
(57) Higashi, G. S.; Chabal, Y. J.; Trucks G. W.; Raghavachari, K. *Appl. Phys. Lett.* **1990**, *57*, 656−658.
(58) Higashi, G. S.; Berker, R. S.; Chabal, Y. J.; Becker A. J. *Appl. Phys. Lett.* **1990**, *58*, 1656−1658.
(59) Jakob, P.; Chabal, Y. J. *J. Chem. Phys.* **1991**, *95*, 2897−2909.
(60) Wade C. P.; Chidsey, C. E. D. *Appl. Phys. Lett.* **1997**, *71*, 1679−1681 (Erratum: **1998**, *72*, 133).

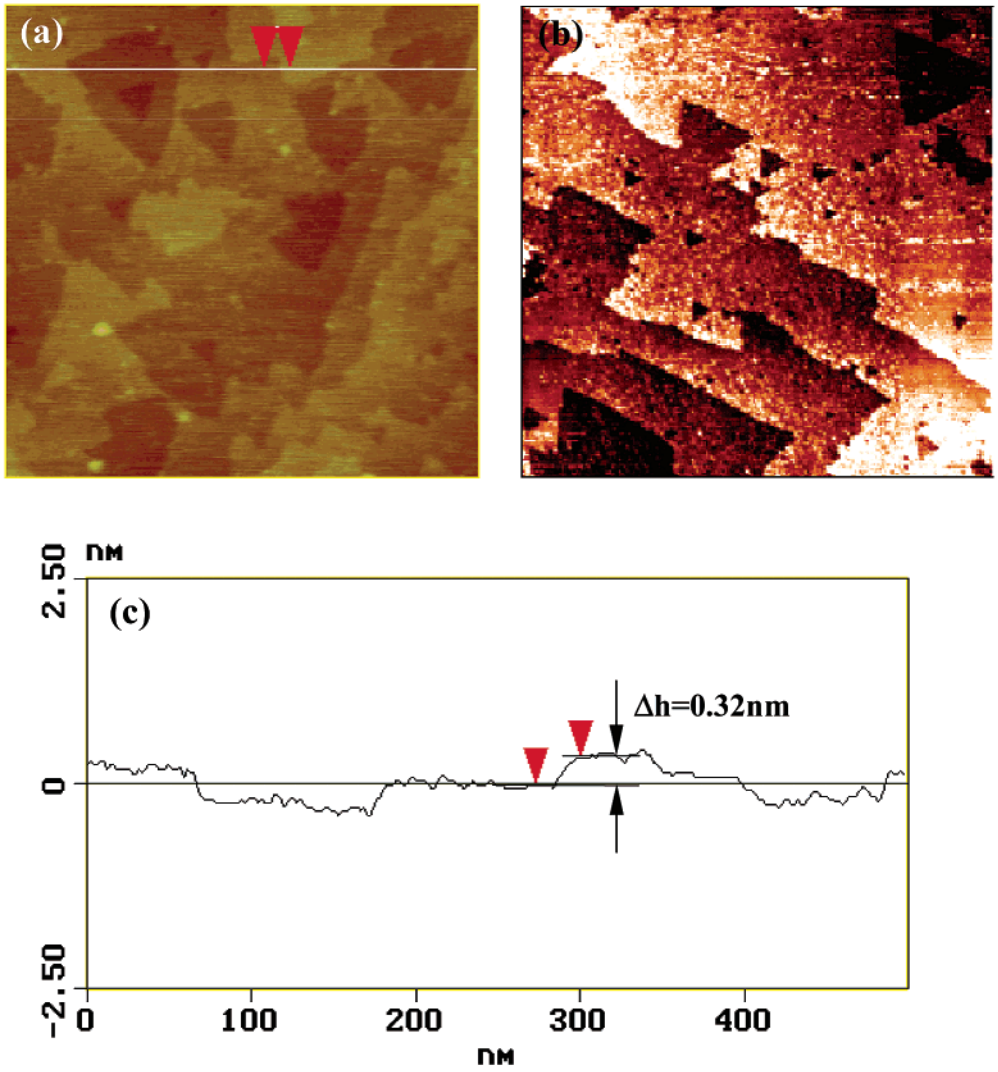

Figure 2. (a) AFM and (b) STM images (500 nm × 500 nm) of a H−Si(111) surface etched in a 40% NH_4F aqueous solution degassed by N_2. (c) A distance of 0.32 nm between two Si(111) terraces found from a section analysis of the AFM image. The gap voltage for STM was −2.1 V.

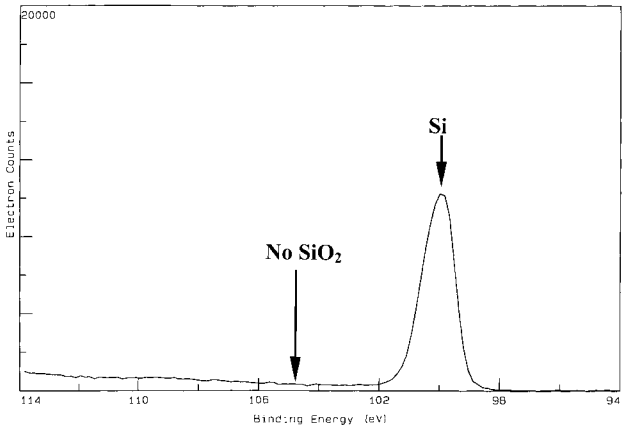

Figure 3. XPS spectrum of Si(2p) for a H−Si(111) surface etched in 40% NH_4F aqueous solution for 5 min. The spectrum remained the same for the sample exposed to air for 24 h.

solution immediately after etching for monolayer preparation. An XPS spectrum for the H-terminated surface is shown in Figure 3. As can be seen, no oxidation peak was found at ∼104 eV. Contaminants were not detected by XPS possibly due to the removal of surface contaminants under high vacuum in XPS experiments but were observed by AFM after the surface was exposed to air. Furthermore, no oxides were found from the XPS spectrum of the H−Si surface exposed to air for 24 h. This indicated that the silicon surface is passivated by the hydrogen-terminated layer.[1]

Alkyl Monolayers on Si(111). Monolayers $-CH_{3,Si}$ and $-COOCH_{3,Si}$ were formed by a thermal hydrosilylation reaction from 1-dodecene and undecylenic acid methyl ester, respectively, while the monolayer $-COOH_{Si}$ was prepared by a hydrolysis reaction of the monolayer $-COOCH_{3,Si}$ in the presence of acid. Experimental[5] and molecular simulation[32−34] studies have shown that ∼50% terminated hydrogen atoms on Si(111) were substituted when monolayers formed.

Parts a−c of Figure 4 present AFM images for monolayers $-CH_{3,Si}$, $-COOCH_{3,Si}$, and $-COOH_{Si}$, respectively. Similar to the H−Si surface as shown in Figure 2, large atomically flat terraces were found on these images. Figure 5 presents XPS spectra of C(1s) for monolayers $-COOCH_{3,Si}$ and $-COOH_{Si}$. One can find a small peak at ∼287 eV, which corresponds to the ester group $-COOCH_3$. For the monolayer $-COOH_{Si}$, the peak at 287 eV disappeared, which indicates that the ester group in the monolayer $-COOCH_{3,Si}$ was converted into a carboxyl group after hydrolyzing in boiling acid for 1 h. It was found that a longer period of hydrolyzing time has no significant

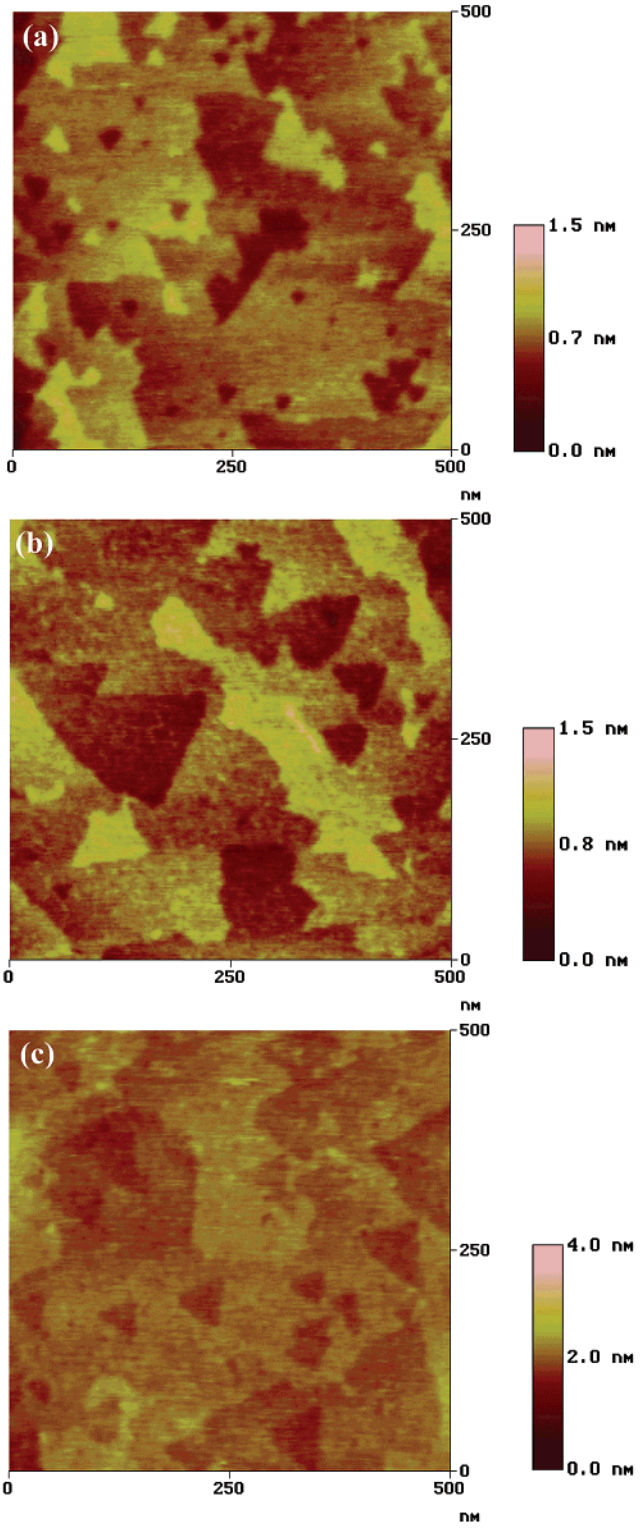

Figure 4. AFM images of monolayers (a) $C_{11}-CH_3/Si$, (b) $C_{10}-COOCH_3/Si$, and (c) $C_{10}-COOCH_3/Si$.

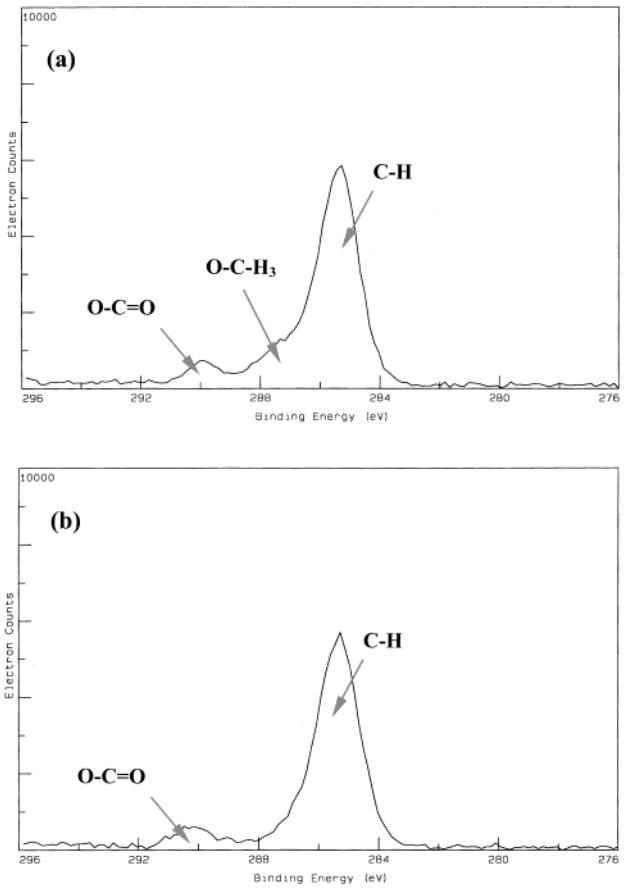

Figure 5. XPS spectra of C(1s) for monolayers (a) $C_{10}-COOCH_3/Si$ and (b) $C_{10}-COOH/Si$.

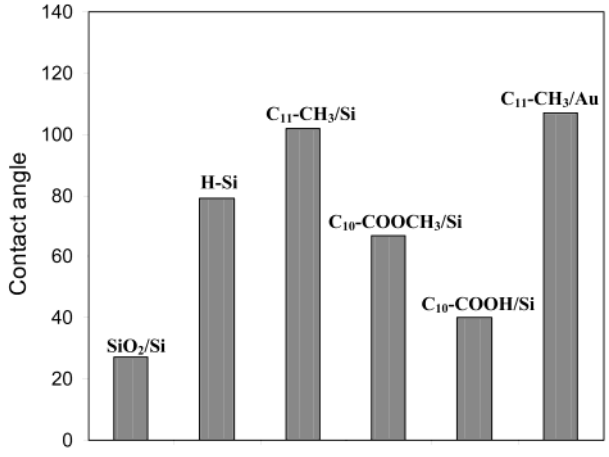

Figure 6. Advancing water contact angles for various surfaces.

influence on the properties of the monolayer $-COOH_{Si}$. A similar effect of the hydrolyzing time on the resulting monolayers was also found by Zuilhof and co-workers.[8]

Advancing water contact angles of the monolayers are shown in Figure 6. For comparison, contact angles for native oxide Si(111) (SiO_2/Si), H−Si, and $-CH_{3,Au}$ are also plotted in Figure 6. The contact angle for the monolayer $-CH_{3,Si}$ (103°) is very close to that for the monolayer $-CH_{3,Au}$ (107°). A native oxide silicon surface has a 27° contact angle. When it was covered by monolayers $-COOH_{Si}$, $-COOCH_{3,Si}$, and $-CH_{3,Si}$, respectively, the contact angle increased, as shown in Figure 6. For the monolayer $-COOH_{Si}$, the contact angle was 48°. Due to reorganization of the monolayer, it is likely that CH_2 groups are exposed at the top.[8]

Figure 7 shows a survey scan spectrum of the monolayer $-CH_{3,Si}$. Only three elements (C, O, and Si) were detected on the surfaces (hydrogen cannot be detected by XPS). This indicates that alkyl monolayers were formed without contaminants of other elements. Figure 8a presents the spectrum of Si(2p) for the monolayers $-CH_{3,Si}$, and no oxidation peak around 104 eV was found from the spectrum. Moreover, the spectrum remained the same for the sample stored in air for 22 days. The XPS spectra in Figure 8 show no peak for C═C bonds, indicating that no

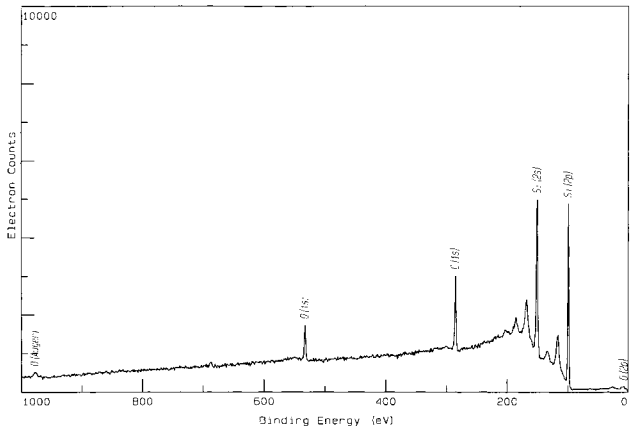

Figure 7. XPS spectra of a survey scan for the monolayer $C_{11}-CH_3$/Si.

precursor molecule existed on the surface to form multilayers. Sieval et al.[8] also found that there was no oxidation formation after the monolayer $-CH_{3,Si}$ was stored under atmospheric conditions at room temperature for 4 months. Spectra b and c of Figure 8 show spectra of Si(2p) for monolayers $-COOCH_{3,Si}$ and $-COOH_{Si}$, respectively. An oxide peak was found at ~104 eV for both cases. The possible sources for the oxide peak are from (i) oxidants in precursors, (ii) dissolved oxygen in etching solution, and (iii) oxygen penetrating into monolayers from air. XPS spectra for these two samples stored in air for 3 weeks remained unchanged (results not shown here), indicating that monolayers $-COOCH_{3,Si}$ and $-COOH_{Si}$ are as stable as the monolayer $-CH_{3,Si}$. This rules out the possibility that oxygen molecules penetrate into monolayers from air. It is expected that dissolved oxygen in precursor solution was removed after the solution was degassed by N_2 for 1−2 h. The same procedure was applied to prepare monolayers $-CH_{3,Si}$ and $-COOCH_{3,Si}$. No oxidation peak observed for the monolayer $-CH_{3,Si}$ rules out the possibility of dissolved oxygen in solution. It is speculated that oxidants contained in the precursor may be responsible for the oxidation peak. However, the quality of the monolayers for passivating silicon surfaces was not affected by the oxidation peak as evidenced by the fact that no further oxidation was observed for the samples stored in air within 3 weeks.

3.2. Frictional and Pull-Off Forces. Nanoscale friction and pull-off forces for surfaces ranging from hydrophobic to hydrophilic (i.e., $-CH_{3,Si}$, $-COOCH_{3,Si}$, and $-COOH_{Si}$) were measured using SFM. For comparison, native oxide Si(111) surface (SiO_2/Si), H−Si, and $-CH_{3,Au}$ were also studied. As one knows, friction is affected not only by surface properties but also by environmental conditions, such as relative humidity.[50−52,61,62] Thus, the effect of humidity on friction and pull-off forces was also investigated.

Figure 9 shows that measured frictional forces for hydrophobic monolayers $-CH_{3,Si}$ and $-COOCH_{3,Si}$ changes with normal load linearly (in air, relative humidity was ~30%). At lower loads, the Hertzian contact model in the elastic regime predicts a $L^{2/3}$ law for a spherical tip and a $L^{1/2}$ law for a conical tip.[63] At higher loads, the change of frictional force vs normal load is no longer linear because

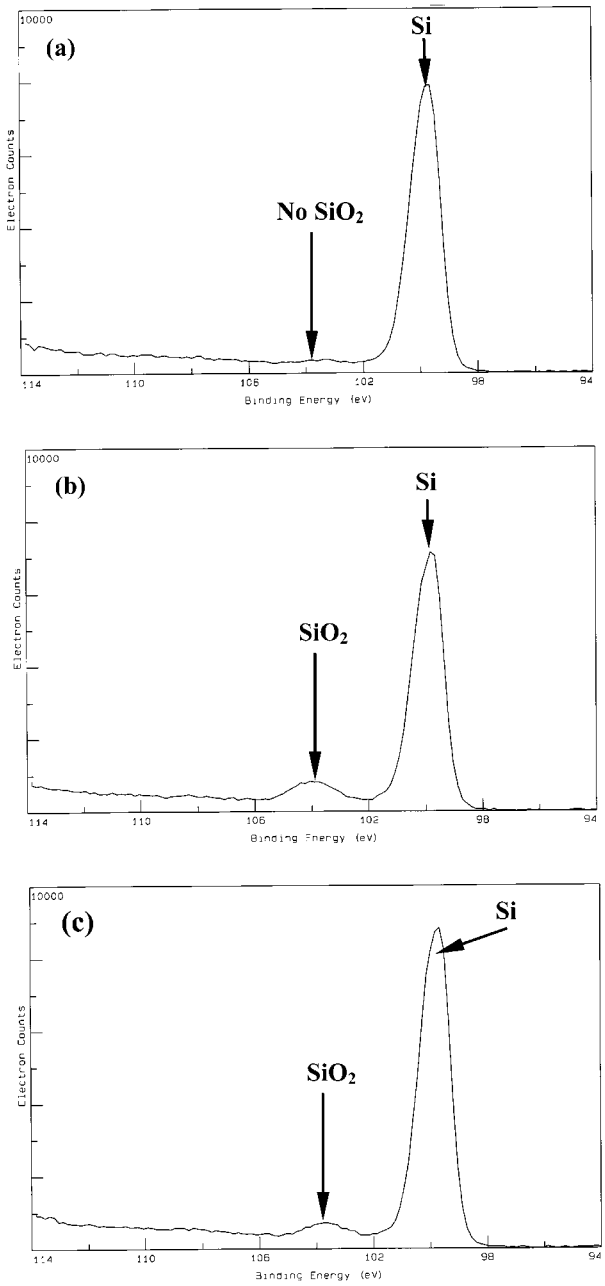

Figure 8. XPS spectra of Si (2p) for monolayers (a) $C_{11}-CH_3$/Si, (b) $C_{10}-COOCH_3$/Si, and (c) $C_{10}-COOH$/Si. The spectra remained the same for these monolayers exposed to air for 3 weeks.

of the occurrence of wear. For the monolayer $-CH_{3,Si}$, two sets of measurements were made. It can be seen from Figure 9 that two lines from different sets of experimental measurements have very close slopes (0.059 and 0.060), indicating that with the same tip, the measurements are reproducible for the same monolayer. A friction coefficient of 0.088 for the monolayer $-CH_{3,Au}$ measured in this work is in good agreement with that of 0.081 measured by Li et al.[38] Since a tip of the same type was used for the measurements, the calibrated value of α/β (38.5)[38] was used to calculate frictional forces in this work. The friction of a native oxide silicon surface is also given in Figure 9 as a reference.

Figure 10 compares friction forces for different monolayers ranging from hydrophilic to hydrophobic with those of a native oxide silicon surface (SiO_2/Si) and H−Si (in air, relative humidity was ~30%). For SiO_2/Si, a friction

(61) Scherge, M.; Li, X.; Schaefer, J. A. *Tribol. Lett.* **1999**, *6*, 216−220.
(62) Quon, R. A.; Ulman, A.; Vandrlick, T. K. *Langmuir* **2000**, *16*, 8912−8916.
(63) Hu, J.; Xiao, X.; Ogletree, D. F.; Salmeron, M. *Surf. Sci.* **1995**, *327*, 358−370.

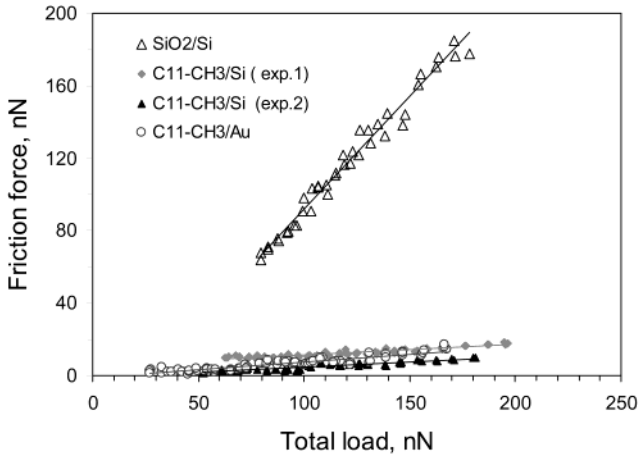

Figure 9. Frictional forces as a function of total loads for different surfaces by scanning force microscopy. For the monolayer $C_{11}-CH_3/Si$, two sets of measurements were made for testing reproducibility (Relative humidity, ~30%).

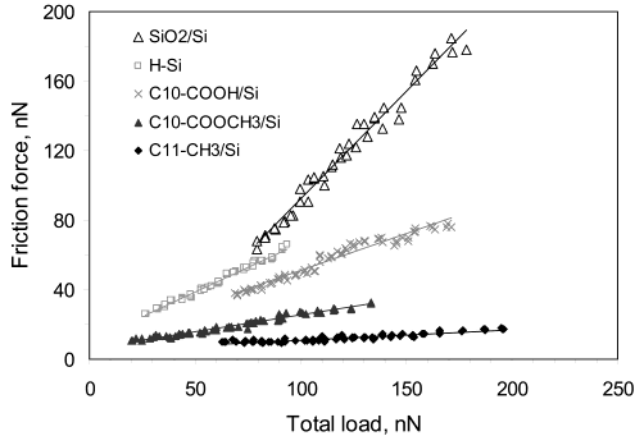

Figure 10. Frictional forces as a function of total loads for different surfaces on Si(111) by scanning force microscopy. Friction coefficient decreases significantly when Si(111) surfaces are modified with different monolayers (relative humidity ~30%).

coefficient of 1.236 was obtained. When the native oxide silicon surface was coated by the monolayers $-COOH_{Si}$, $-COOCH_{3,Si}$, and $-CH_{3,Si}$, friction coefficients decreased to 0.424, 0.194, and 0.060, respectively. These measurements show that friction on a silicon surface could be reduced by 3 times for coating with the hydrophilic monolayer $-COOH_{Si}$, or by 20 times for coating with the hydrophobic monolayer $-CH_{3,Si}$. For H−Si, the measured friction coefficient is 0.571. Although the H−Si surface has been found to be a passivation layer[1] with a water contact angle of 79° measured in this work, the friction of the surface is comparable to that of the hydrophilic monolayer $-COOH_{Si}$. Previous experiments[38−40,51] show that friction coefficient depends not only on terminal group but also on chain length. Although Si−H has a contact angle of 79°, the friction coefficient is quite high due to its short chain. For a summary, friction coefficients for various surfaces are shown in Figure 11. As can be seen, friction decreases in this order: $SiO_2/Si > -COOH_{Si} > -COOCH_{3,Si} > -CH_{3,Si} \sim -CH_{3,Au}$. Results show that friction coefficient decreases as surface property changes from hydrophilic to hydrophobic and that the monolayers terminated by $-CH_3$ on different substrates have similar friction properties.

To study the effect of relative humidity on friction, frictional forces for monolayers $-CH_{3,Si}$, $-COOCH_{3,Si}$, and

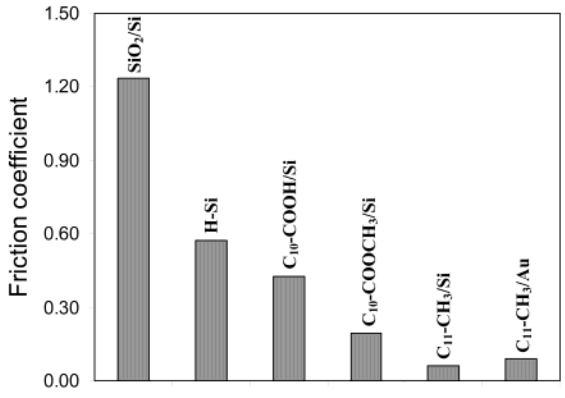

Figure 11. Friction coefficients of various surfaces in air (temperature ~24 °C and relative humidity ~30%) from scanning force microscopy.

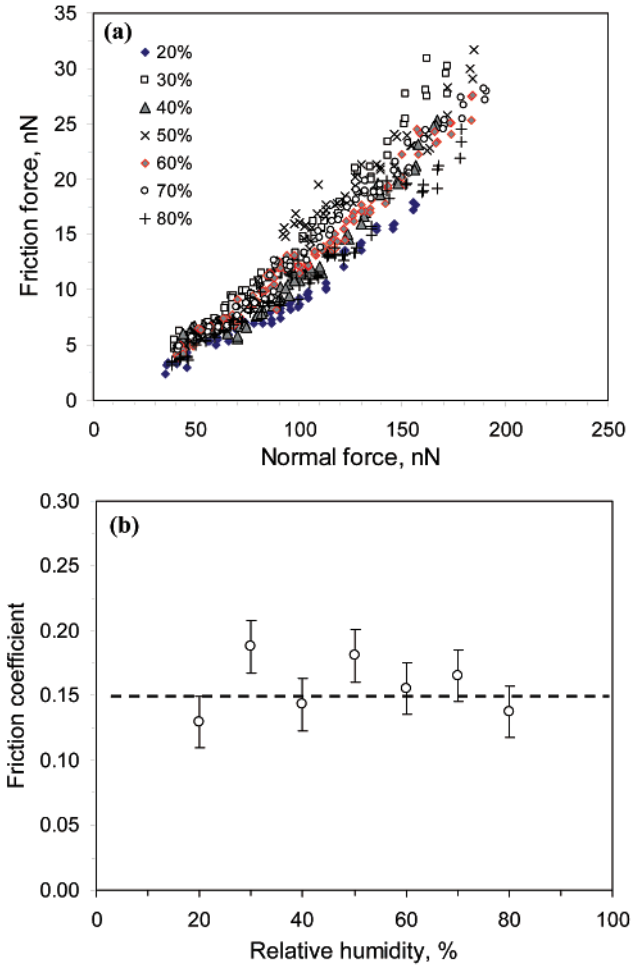

Figure 12. (a) Frictional forces and (b) friction coefficients for the monolayer $C_{11}-CH_3/Si$ under different relative humidities by scanning force microscopy. The broken line in (b) serves only as viewing aids.

$-COOH_{Si}$ were measured under different relative humidities between 10% and 80%. Figure 12 presents frictional forces of the monolayer $-CH_{3,Si}$ as a function of load at various relative humidities. Results show that friction coefficient is not sensitive to humidity for hydrophobic monolayers. The behavior of $-COOCH_{3,Si}$, shown in Figure 13, is similar to that of $-CH_{3,Si}$. Hydrophilic monolayer $-COOCH_{3,Si}$, however, has different behavior. As shown in Figure 14, when relative humidity changed from 20% to 80%, friction coefficient decreased by ~50%.

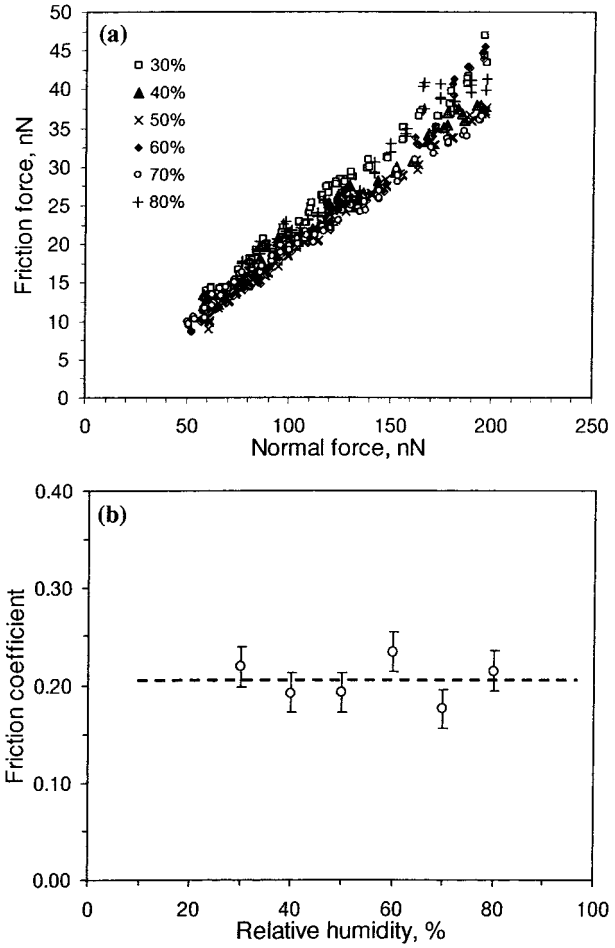

Figure 13. (a) Frictional forces and (b) friction coefficients for the monolayer $C_{10}-COOCH_3/Si$ under different relative humidities from scanning force microscopy. The broken line in (b) serves only as viewing aids.

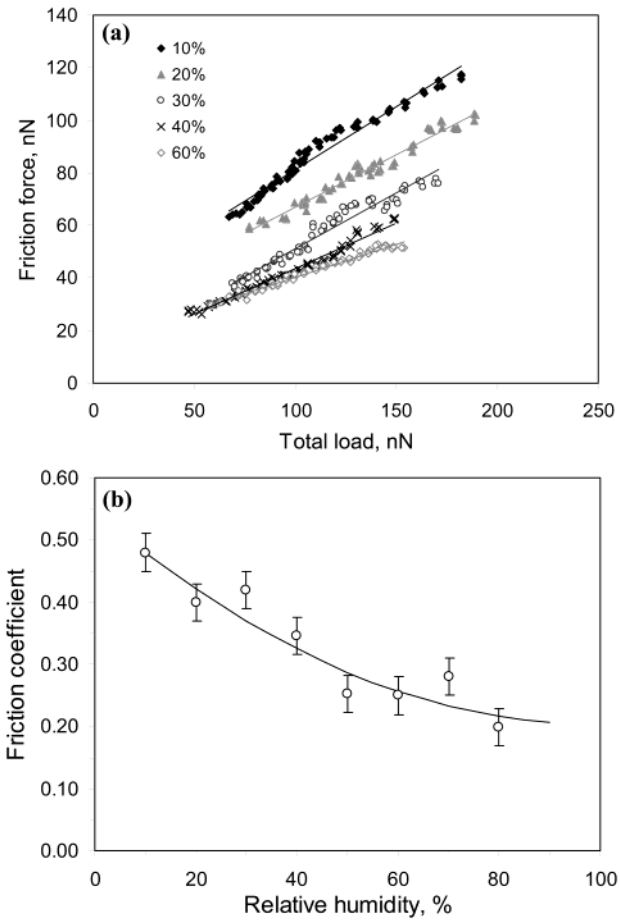

Figure 14. (a) Frictional forces and (b) friction coefficients for the monolayer $C_{10}-COOH/Si$ under different relative humidities from scanning force microscopy. Frictional forces at 50, 70, and 80% are removed from (a) for clarity. The solid line in (b) serves only as viewing aids.

Freund et al.[64] found that when humidity increased, the number of adsorbed water molecules on the monolayer became more, resulting in thick water layers. Experimental measurements have shown that the multiple layers of water molecules on hydrophilic surfaces function as a lubricant.[61] From Figures 12b, 13b, and 14b, it can be seen that the friction coefficient decreases for hydrophilic monolayers while it remains the same for hydrophobic monolayers as relative humidity increases.

Figure 15 presents pull-off forces for various monolayers on Si(111) at different relative humidities. For the hydrophobic surface ($-CH_{3,Si}$), pull-off force is not sensitive to humidity changes, whereas it showed a strong dependence on humidity for the hydrophilic surface ($-COOH_{Si}$). Our results show that there is a flat response in pull-off force for the hydrophilic force at humidities less than 50% and a dramatic increase after 60%. For the monolayer $-COOCH_{3,Si}$, the pull-off force seems to be somewhere between those for the monolayers $-CH_{3,Si}$ and $-COOH_{Si}$ at a variety of humidities, but the effect of humidity on pull-off force for $-COOCH_{3,Si}$ is much smaller than that for $-COOH_{Si}$. The recent work by He et al.[65] showed a similar behavior of pull-off forces for both hydrophilic and hydrophobic surfaces in the range of humidities studied (<80%). The flat response in pull-off force followed by a

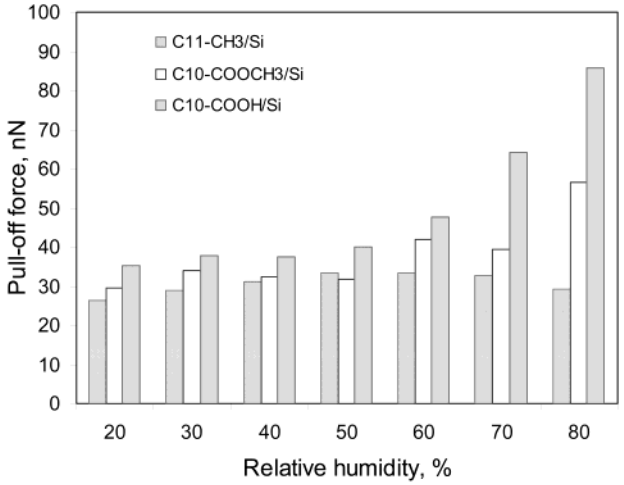

Figure 15. Pull-off forces for various monolayers at a variety of relative humidities from scanning force microscopy.

dramatic increase was also observed on mica surfaces by Salmeron and co-workers,[66] Sedin and Rowlen,[67] and Thundat et al.[68] The transition point from flat response

(64) Freund, J.; Halbritter, J.; Horber, J. K. H. *Microsc. Res. Technol.* **1999**, *44*, 327−338.
(65) He, M.; Blum, A. Z.; Aston, D. E.; Buenviaje, C.; Overney, R. M. *J. Chem. Phys.* **2001**, *114*, 1355−1360.
(66) Xu, L.; Lio, A.; Hu, J.; Ogletree, D. F.; Salmeron, M. *J. Phys. Chem. B* **1998**, *102*, 540−548.
(67) Sedin, D. L.; Rowlen, K. L. *Anal. Chem.* **2000**, *72*, 2183−2189.
(68) Thundat, T.; Zheng, X. Y.; Chen, G. Y.; Warmack R. J. *Surf. Sci.* **1993**, *294*, L939−L943.

to dramatic increase in pull-off force was near 20% relative humidty due to different surfaces used.

4. Conclusions

Alkyl monolayers with different terminal groups of $-CH_3$ and $-COOCH_3$ on Si(111) surfaces were prepared by a direct thermal hydrosilylation reaction between alkenes and H−Si(111) surfaces through Si−C linkage. The −COOH-terminated monolayer was generated from the $-COOCH_3$-terminated monolayer by a hydrolysis reaction in the presence of acid. The H−Si(111) surfaces with large and atomically flat terraces were formed by etching in a degassed 40% NH_4F aqueous solution. The H−Si(111) surfaces and the monolayers were characterized by AFM, STM, contact angle goniometry, and XPS. The monolayers were stable, and no oxidation was observed when the monolayers were exposed to air for about 3 weeks.

Quantitative nanoscale frictional and pull-off forces were measured using scanning force microscopy for H−Si(111), native oxide Si(111) (SiO_2/Si), and C_{12}-thiol on Au(111) at ambient conditions and for the monolayers $-CH_{3,Si}$, $-COOCH_{3,Si}$, and $-COOH_{Si}$ at a variety of relative humidities. The magnitude of the nanoscale frictional force was found to decrease in the order $SiO_2/Si > -COOH_{Si} > -COOCH_{3,Si} > -CH_{3,Si} \sim -CH_{3,Au}$. Compared to the results for SiO_2/Si, the friction coefficient decreases dramatically by 20 times for the hydrophobic monolayer $-CH_{3,Si}$ and by 3 times for the hydrophilic monolayer $-COOH_{Si}$. The monolayers terminated with $-CH_3$ on different substrates have similar friction properties. With increase of relative humidity, frictional force remains the same for hydrophobic monolayers, whereas it decreases for hydrophilic monolayers. Pull-off force is not sensitive to relative humidity for hydrophobic monolayers $-CH_{3,Si}$ and $-COOCH_{3,Si}$, whereas it depends on relative humidity for the hydrophilic monolayer $-COOH_{Si}$ at humidities greater than 60%.

Acknowledgment. The authors thank the National Science Foundation CTS-0092699 (CAREER Award) and CMS-9988745 for financial support.

LA011718A